Elastic Moduli Inheritance and the Weakest Link in Bulk Metallic Glasses

D. Ma,[1] A. D. Stoica,[1] X.-L. Wang,[1,*] Z. P. Lu,[2] B. Clausen,[3] and D. W. Brown[3]

[1]*Neutron Scattering Science Division, Oak Ridge National Laboratory, Oak Ridge, Tennessee, USA*
[2]*State Key Laboratory for Advanced Metals and Materials, University of Science and Technology Beijing, Beijing, China*
[3]*Lujan Neutron Scattering Center, Los Alamos National Laboratory, Los Alamos, New Mexico, USA*

(Received 8 May 2011; published 22 February 2012)

We show that a variety of bulk metallic glasses (BMGs) *inherit* their Young's modulus and shear modulus from the solvent components. This is attributed to preferential straining of locally solvent-rich configurations among tightly bonded atomic clusters, which constitute the weakest link in an amorphous structure. This aspect of inhomogeneous deformation, also revealed by our *in situ* neutron diffraction studies of an elastically deformed BMG, suggests a rubberlike viscoelastic behavior due to a hierarchy of atomic bonds in BMGs.

DOI: 10.1103/PhysRevLett.108.085501 PACS numbers: 62.20.de, 61.05.fm, 62.20.dj, 62.20.dq

While limited plasticity has been the Achilles' heel of bulk metallic glasses (BMGs) over the years, the superior elastic limit of ~2% is a hallmark of these materials for structural applications [1]. However, compared with tremendous efforts being made for understanding the plasticity, very little is known about what happens microscopically prior to yielding and what is the structural origin of the unusually large elastic limit [2]. Conventionally, the elasticity of a glass is viewed as what takes place in an isotropic solid, i.e., elastic bond stretching and uniform straining at all scales. This conventional wisdom is now challenged by high-energy x-ray diffraction studies which have demonstrated that microscopic strains in a BMG are indeed dependent on the length scales: more distant atomic shells are less stiffer than the nearest-neighbor shell upon loading [3–5]. Poulsen *et al.* [3] postulated that this is because of structural rearrangement at the medium-range scale of 4–10 Å, whereas Hufnagel *et al.* [4] proposed that it is due to local atomic rearrangements in topologically unstable regions of the amorphous structure. Dmowski *et al.* [5] further suggested that about a quarter in volume fraction of a BMG is anelastic which represents residual liquidity. These debates indicate that a physical understanding of the microscopic deformation mechanism is still unsettled. In this Letter, we set out to investigate the elasticity by examining Young's modulus (E) and the shear modulus (G) for a variety of BMGs, and observed, surprisingly, that they essentially *adopt* the moduli of their solvent (or ''base metal'') components. We attribute this to preferential straining of solvent-rich configurations, which is supported by our *in situ* loading neutron diffraction studies of a Zr-based BMG.

Table I summarizes experimental data of E and G for BMGs based on Zr, Mg, La, Ce, Er, Pr, Dy, Fe, and Au, respectively, along with those of their solvent components [1,6–14]. It is striking to see that both E and G values of these BMGs are very close to those of the solvent components. This is unusual because solvent atoms make up only about 50% of such a glass, but appear to be responsible for the overall stiffness and rigidity. For instance, the Young's modulus (E) of Vitreloy 1 ($Zr_{41.2}Ti_{13.8}Ni_{10}Cu_{12.5}Be_{22.5}$, the best metalloid-free BMG) is 97.2 GPa [7], almost identical to that of pure polycrystalline Zr (98.0 GPa) [6]; whereas, this value is much smaller than those of other components, i.e., 120.2 GPa of Ti, 129.8 of Cu, 199.5 GPa of Ni, and 318 GPa of Be. As for shear modulus (G), Vitreloy 1 has a value of 35.0 GPa, which is also nearly the same as that of Zr (35.9 GPa) but significantly smaller than those of Ti (45.6 GPa), Cu (48.3 GPa), Ni (76.0 GPa), and Be (156 GPa). The average value of E of the BMGs listed in Table I is found to be ~97% of that of the solvent components, while for G, the ratio is ~96%. Considering that most of the data were obtained by ultrasonic measurements for which the experimental error is ~5% [8], one can conclude that the elastic moduli of these BMGs are *primarily* determined by their solvent components. Since the elastic modulus reflects the inherent stiffness of atomic bonds [4], Table I suggests that solvent-solvent bonds are essentially responsible for the elasticity of BMGs. A corollary is that, despite the chemical and structural complexity of the BMGs, the more compliant solvent-solvent bonds are sustaining the majority of strain upon deformation.

Previous experiments showed that a BMG is generally 30% softer, in terms of E and G, than its crystalline counterpart (i.e., a devitrified BMG) [15,16]. Interestingly, the moduli of a devitrified BMG can be very well approximated by a constant-stress or Reuss type of ''rule of mixtures'' [8,16]: $C = 1/(\sum_i f_i/C_i)$ where C represents E or G, f_i is the atomic fraction of the ith component, and C_i is E or G of the ith component. For instance, the E and G of the devitrified Vitreloy 1 have been measured to be 128.7 and 48.8 GPa, respectively [16], which agree very well with the ''rule of mixtures'' values of 130.9 and 49.6 GPa. This *rule-of-mixture* principle also appears to hold in other devitrified BMGs such as $Pr_{60}Ni_{10}Al_{10}Cu_{20}$ [16] and $Ce_{70}Cu_{10}Ni_{10}Al_{10}$ [8]. These

TABLE I. Experimental Young's modulus (E) and shear modulus (G) for BMGs and their solvent elements (Sol). Also listed are the ratios of BMG to solvent in terms of E and G, respectively. Data for solvents were taken from [6].

BMGs	Sol	E (GPa)			G (GPa)			Ref.
		BMG	Sol	Ratio	BMG	Sol	Ratio	
$Zr_{55}Cu_7Co_{19}Al_{19}$	Zr	101.7	98.0	1.04	37.6	35.0	1.07	[1]
$Zr_{41.2}Ti_{13.8}Ni_{10}Cu_{12.5}Be_{22.5}$	Zr	97.2	98.0	0.99	35.9	35.0	1.03	[1]
$Zr_{48}Nb_8Cu_{12}Fe_8Be_{24}$	Zr	95.7	98.0	0.98	35.2	35.0	1.01	[7]
$Zr_{48}Nb_8Cu_{14}Ni_{12}Be_{18}$	Zr	93.9	98.0	0.96	34.3	35.0	0.98	[7]
$Zr_{46}Cu_{46}Al_8$	Zr	93.7	98.0	0.96	34.3	35.0	0.98	[8]
$Zr_{50.6}Ti_{5.1}Cu_{18.9}Ni_{11.1}Al_{14.3}$	Zr	92.7	98.0	0.95	34.0	35.0	0.97	[7]
$Zr_{50}Cu_{50}$	Zr	85.0	98.0	0.87	31.3	35.0	0.89	[8]
$Zr_{55}Ti_5Cu_{20}Ni_{10}Al_{10}$	Zr	85.0	98.0	0.87	31.0	35.0	0.89	[8]
$Zr_{57.5}Nb_5Cu_{15.5}Ni_{12}Al_{10}$	Zr	84.7	98.0	0.86	30.8	35.0	0.88	[7]
$Er_{50}Y_6Al_{24}Co_{20}$	Er	71.1	70.0	1.02	27.0	28.0	0.96	[8]
$Ho_{39}Al_{24}Co_{20}Y_{12}Zr_5$	Ho	69.3	65.0	1.07	26.2	26.0	1.01	[9]
$Ho_{39}Al_{25}Co_{20}Y_{16}$	Ho	69.1	65.0	1.06	26.2	26.0	1.01	[9]
$Dy_{46}Y_{10}Al_{24}Co_{18}Fe_2$	Dy	64.2	61.0	1.05	24.4	25.0	0.98	[10]
$Mg_{65}Cu_{25}Gd_{10}$	Mg	49.1	44.7	1.10	18.6	17.3	1.08	[1]
$La_{55}Cu_{10}Ni_5Co_5Al_{25}$	La	41.9	37.9	1.11	15.6	14.9	1.05	[8]
$La_{66}Cu_{10}Ni_{10}Al_{14}$	La	35.7	37.9	0.94	13.4	14.9	0.90	[8]
$La_{62}Cu_{11.7}Ag_{2.3}Ni_5Co_5Al_{14}$	La	35.0	37.9	0.92	13.0	14.9	0.87	[11]
$Pr_{60}Ni_{10}Al_{10}Cu_{20}$	Pr	37.2	37.0	1.01	13.6	15.0	0.91	[10]
$Ce_{68}Cu_{20}Nb_2Al_{10}$	Ce	31.0	33.5	0.93	12.0	13.5	0.89	[12]
$Ce_{68}Cu_{20}Fe_2Al_{10}$	Ce	30.8	33.5	0.92	11.8	13.5	0.87	[8]
$Ce_{70}Cu_{10}Ni_{10}Al_{10}$	Ce	30.3	33.5	0.90	11.5	13.5	0.85	[10]
$Fe_{61}Mn_{10}Cr_4Mo_6Er_1C_{15}B_6$	Fe	193	211.4	0.91	75	81.6	0.92	[13]
$Fe_{53}Cr_{15}Mo_{14}Er_1C_{15}B_6$	Fe	195	211.4	0.92	75	81.6	0.92	[13]
$Au_{49.5}Ag_{5.5}Pd_{2.3}Cu_{26.9}Si_{16.3}$	Au	74.4	78.5	0.95	26.5	26	1.02	[14]
$Au_{55}Cu_{25}Si_{20}$	Au	69.8	78.5	0.89	24.6	26	0.95	[14]
Mean				0.97			0.96	
Standard Deviation				0.07			0.07	

results show that every component in a *devitrified* BMG contributes its part of stiffness (weighted by fraction) to the overall modulus. In other words, atomic bonds in the crystalline state are subjected to homogeneous deformation. This, being distinct from what we observed for BMGs as discussed above, provides further evidence for preferential straining of solvent-solvent bonds upon deforming a BMG.

To explore the structural origin of this unusual aspect of elasticity, we have carried out an *in situ* neutron diffraction study of a Zr-based BMG ($Zr_{52.5}Cu_{17.9}Ni_{14.6}Al_{10}Ti_5$) uniaxially compressed up to ~70% of its elastic limit using the SMARTS diffractometer at Los Alamos National Laboratory. A cylindrical sample (6.6 mm dia. and 14.0 mm long) made from a copper-mould cast Zr-BMG rod was used for the *in situ* experiment, in which neutron diffraction data were collected for 2 hours at each stress level of 10, 500, 1000, and 1500 MPa during loading, as well as at 10 MPa after unloading. The momentum transfer, $q = 4\pi \sin\theta/\lambda$, is up to 20.0 Å^{-1} where 2θ is the diffraction angle and λ is the neutron wavelength. The total structure factors $S(q)$, with respect to longitudinal and transverse directions, were obtained using the program PDFgetN [17], with absorption corrections accounting for the horizontal loading geometry.

Figure 1(a) shows the experimental $S(q)$-s with respect to the longitudinal direction under four compressive stresses of 10, 500, 1000, and 1500 MPa, respectively. The difference curves are shown in Fig. 1(b). For a given peak, a negative-positive sequence in the difference plot means that the peak shifts to higher q under load. One can see that, with an increase in stress, the first diffraction peak shifts consistently toward higher q values, with essentially no change in the peak shape. In contrast, changes in the high q portion of $S(q)$, particularly beyond the 2nd peak (~ 6 Å^{-1}), are much smaller. Meanwhile, the transverse $S(q)$ (not shown) exhibits an opposite trend on the shift of the first peak in response to stress, but behaves similarly for the high-q portion. It is also noted that the $S(q)$ fully recovered after unloading, indicative of the apparently elastic nature of the deformation.

The change of $S(q)$ in response to stress provides a basis for the determination of microscopic strains. Here, we consider that the elastic strain induces only a scale change

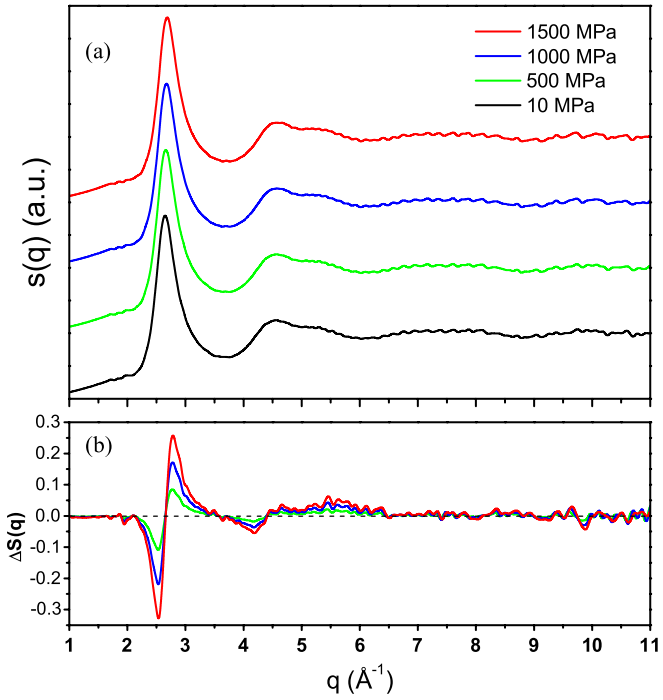

FIG. 1 (color online). (a) The longitudinal structure factor $S(q)$ under a compressive stress of 10, 500, 1000, and 1500 MPa, respectively. (b) Difference plot of $S(q)$-s, between 10 MPa and higher stress levels.

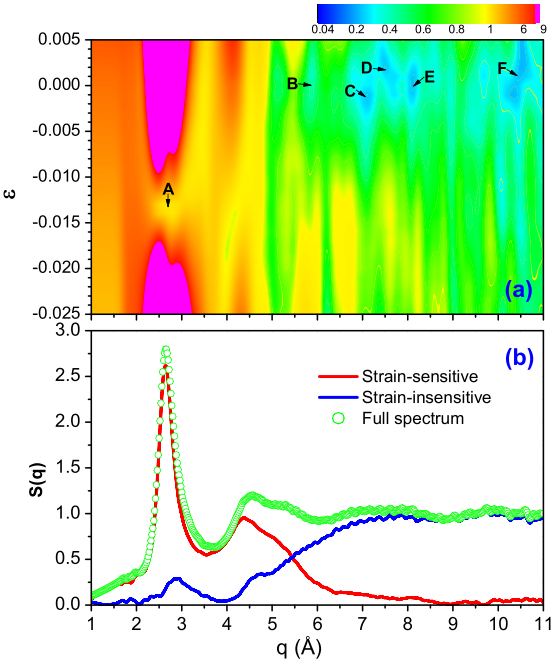

FIG. 2 (color online). (a) A χ^2-type functional $\Delta[\varepsilon, q]$ between two $S(q)$-s corresponding to stresses of 10 and 1500 MPa, as a function of ε and q, showing the q-dependent strains. Letters (A–F) point to local minima. (b) Decomposition of the structure factor obtained under the initial loading condition into the strain-sensitive and strain-insensitive partials.

in q rather than a change in the shape of $S(q)$. Thus, we define a q-dependent strain,

$$\varepsilon = q/q_\sigma - 1 \tag{1}$$

where, unlike being restricted to a peak position as for a polycrystalline material, q refers to *any* value of the momentum transfer related to the structure factor $[S_0(q)]$ obtained under the initial loading condition ($\sigma =$ 10 MPa), and q_σ is the strained value corresponding to the structure factor $[S_\sigma(q_\sigma)]$ under an applied stress (σ). The strain ε was determined by implementing a pattern matching technique, where for a given q value, the $S_0(q)$ curve in the vicinity of q was displaced by $q \cdot \varepsilon$. A χ^2-type functional $\Delta[\varepsilon, q]$ accounting for the difference between $S_\sigma(q_\sigma)$ and $S_0[(1 + \varepsilon)q]$ was evaluated for each trial value of ε, and ε was determined when $\Delta[\varepsilon, q]$ reaches a minimum. Details of this χ^2 method are described in the Supplemental Material [18]. Figure 2 depicts the $\Delta[\varepsilon, q]$ as a contour plot of ε and q, for which $\sigma = 1500$ MPa. Each of the six letters (A–F) in Fig. 2(a) points to a local minimum, which represents the most likely value of the microscopic strain at the corresponding q scale. The A strain is the largest among all ($-$ 1.3%), while the B–F strains are vanishingly small. Thus Fig. 2(a) suggests, in a quantitative way, that the low-q portion of the $S(q)$ responds much more sensitively to stress than the high-q part does. Based on this observation, a simple approach was used to decompose the structure factors into two partials: one is strain sensitive $[S^{\mathrm{el}}(q)]$ and the other is strain insensitive $[S^{\mathrm{in}}(q)]$, given that $S^{\mathrm{el}}(q)$ can be scaled using Eq. (1) with an overall strain value and $S^{\mathrm{in}}(q)$ remains unchanged under stress. Details of the decomposition procedure are described in the Supplemental Material [18]. The analysis results are presented in Fig. 2(b). As expected, $S^{\mathrm{el}}(q)$ covers primarily the low-q spectrum (including the first peak and the beginning of the second peak) and approaches zero at q beyond the second peak, whereas $S^{\mathrm{in}}(q)$ dominates the high-q portion but diminishes in the low-q region (see the estimate of errors in the Supplemental Material [18]).

Despite the lack of long-range crystalline order, metallic glasses are known to exhibit some degrees of short-range order (SRO) and medium-range order (MRO). Previous studies have revealed that SROs are characterized by solute-centered clusters, each of which is made up of a solute atom surrounded by a majority of solvent atoms, and the MRO is constructed by packing of the clusters beyond the SRO [19–21]. As has been discussed by Cargill [22] and later by Suzuki *et al.* [23], the first diffraction peak in $S(q)$ describes the medium-range atomic correlation in real space, while the high-q portion of $S(q)$ reflects the short-range order. Such prior knowledge provides a basis for linking the decomposed partials with atomic configurations in BMGs: the strain-sensitive partial $[S^{\mathrm{el}}(q)]$ describes the MRO, while the strain-insensitive partial

$[S^{in}(q)]$ manifests the SRO, i.e., the solute-centered clusters and/or the superclusters that are made up of, by efficient packing, quasiequivalent solute-centered clusters [19–21]. Thus, the scaling of $S^{el}(q)$ with strain indicates that the MRO is elastically deformed by a uniform strain, while, on the other hand, the insensitiveness of $S^{in}(q)$ to strain suggests that atomic clusters behave in a much stiffer manner. Bearing these in mind while recalling that the elastic moduli of BMGs are essentially determined by solvent-solvent bonding (Table I), one can imagine that deformation in BMG mainly occurs at the junctions among tightly bonded atomic clusters where solvent atoms locally have higher concentrations. In the following, we describe a physical model to interpret this inhomogeneous deformation behavior.

Here we argue that, as shown in Fig. 3, a majority of the junctions among the solute-centered clusters (marked as *B*) and/or the superclusters (marked as *C* which are bounded by solvent atoms in the outmost shell [20]) are occupied by excess solvent atoms (marked as *A*). Such a junction is highly solvent rich and thus characterized primarily by solvent-solvent bonding. As solute-centered clusters are locally efficient packed while a glass is globally less dense than its crystalline counterpart, solvent-rich junctions are likely to be packed loosely. Also, since solvent-solvent bonds are usually the most compliant among the constituents, the solvent-rich junctions constitute the weakest configurations in the amorphous structure. Under an applied load, it is likely that solvent atoms associated with solvent-rich junctions are preferentially strained to accommodate the applied stress. However, macroscopically, local distortion of the solvent-rich junctions results in apparently elastic deformation of neighboring atomic clusters. In this scenario, since solute atoms are in the local center of symmetry and metallic bonds are nondirectional, clusters and/or superclusters may rotate slightly with respect to solute atoms but the solute-solvent distance will be largely unchanged to avoid an energy penalty [24]. This collective response makes atomic clusters (and/or superclusters) behave like molecular units. Consequently, solvent-solvent interactions in the intercluster junctions dictate the ultimate stiffness. This explains why the elastic moduli of a BMG are determined primarily by its solvent component. The small deviation (see Table I) can be attributed to the variation of the bonding characteristics in the intercluster junctions, owing to either the presence of *antisite* solute atoms in the clusters that leads to slightly tighter bonding or the set-in of free volume in the junction which softens the solvent-solvent bonding.

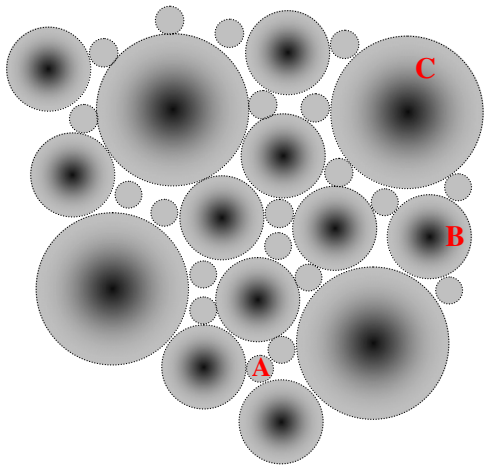

FIG. 3 (color online). Schematic illustration of a hypothetical amorphous structure showing local packing of solvent atoms (*A*), solute-centered clusters (*B*) and superclusters (*C*) in a metallic glass. The gray color in *B* and *C* denotes the outmost atomic shell filled with a majority of solvent atoms. The dark spot in *B* represents the solute atom of a solute-centered cluster, while the dark area in *C* represents the inner solute-enriched region within a supercluster.

The peculiar elasticity of BMGs, while in contrast with that of conventional crystalline metals, is actually analogous to that of rubbery materials [25]. Rubber, as a supercooled liquid, is characterized by two types of bonding forces: very strong interatomic forces bonding the carbon and hydrogen atoms into molecules and much weaker (secondary) van der Waals forces joining the molecules together to form the macroscopic substance. The elasticity of rubber results from the breakdown of some of the intermolecular linkage upon loading, and the flexibility of molecules due to the degree of rotational freedom (i.e., carbon atoms rotating relative to their neighbors but keep the center-to-center distance unchanged) [25]. As a result, rubber exhibits a low modulus of elasticity which reflects the intermolecular interactions due to the van der Waals forces. Analogously, a BMG can be also viewed as being formed by a hierarchy of bonding forces: very strong solute-solvent interactions bonding solute and solvent atoms together to form solute-centered clusters (like molecular units in rubber), and much weaker solvent-solvent bonds linking the clusters (akin to van der Waals forces in rubber). For instance, bonds of Zr-Ni, Zr-Cu, and Zr-Be in Vitreloy 1 are much stronger than Zr-Zr, as indicated by their large negative values of enthalpy of mixing [26], which are -49, -23, and -43 kJ/mol, respectively. In this regard, it is reasonable to conclude that the elasticity of a BMG is primarily determined by its solvent-solvent bonds, as they are the most compliant in the hierarchy of atomic bonds.

In summary, the present study reported new findings that for a variety of bulk metallic glasses, their Young's modulus and shear modulus are essentially identical to those of their base metals and linked this moduli inheritance to the characteristic hierarchical structure of bulk metallic glasses. Since BMGs' elastic strain limits are almost identical ($\sim 2\%$) [1], the intrinsic yield (and/or fracture) strengths of a BMG are also likely dominated by the solvents. This finding may provide guidance for the design

of new BMGs with desirable mechanical properties, and for understanding the nucleation of shear bands, the principal fracture mechanism in metallic glasses.

This research was sponsored by the Laboratory Directed Research and Development Program of Oak Ridge National Laboratory, managed by UT-Battelle, LLC, for the U. S. Department of Energy. The neutron diffraction work was carried out at Lujan Neutron Scattering Center at Los Alamos National Laboratory, sponsored by the Scientific User Facilities Division, Office of Basic Energy Sciences, U.S. Department of Energy. Z. P. L. acknowledges the support from the National Natural Science Foundation of China (No. 51010001), 111 Project (B07003), and the Program for Changjiang Scholars and Innovative Research Team in Universities.

*wangxl@ornl.gov

[1] W. L. Johnson and K. Samwer, Phys. Rev. Lett. **95**, 195501 (2005).
[2] C. A. Schuh, T. C. Hufnagel, and U. Ramamurty, Acta Mater. **55**, 4067 (2007).
[3] H. F. Poulsen *et al.*, Nature Mater. **4**, 33 (2005).
[4] T. C. Hufnagel, R. T. Ott, and J. Almer, Phys. Rev. B **73**, 064204 (2006).
[5] W. Dmowski *et al.*, Phys. Rev. Lett. **105**, 205502 (2010).
[6] E. A. Brandes, *Smithells Metals Reference Book* (Butterworths, London, 2001).
[7] W. H. Wang, C. Dong, and C. H. Shek, Mater. Sci. Eng., R **44**, 45 (2004).
[8] W. H. Wang, J. Appl. Phys. **99**, 093506 (2006).
[9] Q. Luo *et al.*, Appl. Phys. Lett. **88**, 181909 (2006).
[10] S. Li, R. J. Wang, and W. H. Wang, J. Non-Cryst. Solids **352**, 3942 (2006).
[11] Q. K. Jiang *et al.*, Acta Mater. **55**, 4409 (2007).
[12] B. Zhang *et al.*, Phys. Rev. Lett. **94**, 205502 (2005).
[13] V. Ponnambalam, S. J. Poon, and G. J. Shiflet, J. Mater. Res. **19**, 3046 (2004).
[14] J. Schroers *et al.*, Appl. Phys. Lett. **87**, 061912 (2005).
[15] D. Weaire *et al.*, Acta Metall. **19**, 779 (1971).
[16] Z. F. Zhao *et al.*, J. Mater. Res. **21**, 369 (2006).
[17] P. F. Peterson *et al.*, J. Appl. Crystallogr. **33**, 1192 (2000).
[18] See Supplemental Material at http://link.aps.org/supplemental/10.1103/PhysRevLett.108.085501 for details of data analysis and error estimation.
[19] D. B. Miracle, Nature Mater. **3**, 697 (2004).
[20] H. W. Sheng *et al.*, Nature (London) **439**, 419 (2006).
[21] D. Ma, A. D. Stoica, and X. L. Wang, Nature Mater. **8**, 30 (2009).
[22] G. S. Cargill, III, Solid State Phys. **30**, 227 (1975).
[23] Y. Suzuki, J. Haimovich, and T. Egami, Phys. Rev. B **35**, 2162 (1987).
[24] C. Fan *et al.*, Appl. Phys. Lett. **89**, 111905 (2006).
[25] L. R. G. Treloar, *The Physics of Rubber Elasticity* (Oxford University Press, Oxford, 2005).
[26] F. R. de Boer *et al.*, *Cohesion in Metals: Transition Metal Alloys* (North-Holland, Amsterdam, 1988).